Numer. Math. Theor. Meth. Appl.
doi: 10.4208/nmtma.2011.42s.7

Vol. **4**, No. 2, pp. 237-254
May 2011

An Efficient Numerical Method for the Quintic Complex Swift-Hohenberg Equation

Hanquan Wang[1,2,*] and Lina Yanti[2]

[1] *School of Statistics and Mathematics, Yunnan University of Finance and Economics, Kunming, Yunnan Province, 650221, P. R. China.*
[2] *Department of Mathematics, National University of Singapore, 117543, Singapore.*

Received 21 June 2010; Accepted (in revised version) 16 November 2010

Available online 6 April 2011

Abstract. In this paper, we present an efficient time-splitting Fourier spectral method for the quintic complex Swift-Hohenberg equation. Using the Strang time-splitting technique, we split the equation into linear part and nonlinear part. The linear part is solved with Fourier Pseudospectral method; the nonlinear part is solved analytically. We show that the method is easy to be applied and second-order in time and spectrally accurate in space. We apply the method to investigate soliton propagation, soliton interaction, and generation of stable moving pulses in one dimension and stable vortex solitons in two dimensions.

AMS subject classifications: 65M70, 65Z05

Key words: Quintic complex Swift-Hohenberg equation, time-splitting Fourier pseudospectral method, numerical simulation, soliton.

1. Introduction

Swift-Hohenberg equation was proposed by J. Swift and P. C. Hohenberg in 1977 along with the arising interest in stable spatially localized states [18–20]. It has been viewed as a model equation for a large class of higher-order parabolic model equations arising in a wide range of applications, such as the extended Fisher-Kolmogorov equation in statistical mechanics and the perturbed diffusion equation in phase field models [9, 14].

It is undoubtedly convenient if one can use just a single equation to explain a complicated phenomena in various systems. Initially, a single quintic complex Ginzburg-Landau (QCGL) equation was known to be able to do this for a laser with a fast saturable absorber. Its quintic nonlinearity is essential to ensure the stability of soliton-like pulses overcoming something that the cubic Ginzburg-Landau equation could not achieve. However, this

*Corresponding author. *Email addresses:* hanquan.wang@gmail.com (H. Wang), linayanti@nus.edu.sg (L. Yanti)

model is restricted to a second-order term and a spectral response with a single maximum, which is not the case in many experiments. In order to make the model more realistic. the addition of a fourth-order spectral filtering term into the QCGL equation is needed and this is how the quintic complex Swift-Hohenberg equation emerged.

The quintic complex Swift-Hohenberg equation has a wide range of applications. It has been used to study instabilities and pattern formation phenomena in cases of Rayleigh-Bernard convection [4] and oscillating chemical reactions. In optics, this equation has been considered in relation to spatial structures in large aspect lasers [19] and synchronously pumped optical parametric oscillators [20, 29]. It is also important for describing pulse generation processes in passively mode-locked lasers with fast saturable absorbers [30].

The problem which we study numerically is the quintic complex Swift-Hohenberg (QCSH) equation [15, 19, 20, 22–24, 28], expressed as follows

$$i\frac{\partial \psi}{\partial t} = a\psi + b|\psi|^2\psi + c|\psi|^4\psi + d\triangle\psi + f\triangle^2\psi, \qquad \mathbf{x} \in R^d,\ t \geq 0, \tag{1.1}$$

where the function $\psi = \psi(\mathbf{x}, t)$ is a complex wave function with respect to time variable t and space variable $\mathbf{x}$, and a, b, c, d, and f are complex. f is also usually called viscous term in the equation.

Eq. (1.1) covers many nonlinear equations arising in various applications. For example, when a, b, c, d, and f are pure imaginary, it is the real Swift-Hohenberg equation. It has been used to study the collection between subcritical square patterns and oscillons in vertically vibrated granular layers [10] and to describe a wide range of patterns from Ravleigh-Benard convection to wide-area lasers [4]. When $f = 0$, i.e. excluding the viscous term, it collapses to the QCGL equation, which has been studied in many areas, such as fluid dynamics [17], chemical oscillations [18], and nonlinear optics [1]. Furthermore, if all the parameters in the QCGL equation are pure imaginary, it becomes the real Ginzburg-Landau equation. It has been used to examine the interaction of fronts in localized traveling wave pulses in binary liquid mixtures [16]. On the contrary, if the parameters are all real, the equation reduces to the nonlinear Schrödinger equation, which has been used for modeling for example, superfluidity or Bose-Einstein condensation [7].

There has been a lot of studies conducted for the QCSH equation without the viscous term i.e., $f = 0$. For example, stable pulse solutions, namely plain pulse which has the standard soliton shape, narrow composite pulse, and wide composite Pulse, have been found numerically for a wide range of parameters well beyond the region where analytical solutions exist [3]. The interactions between the more complicated structure of the composite pulses have been studied, too. Through numerical simulation, collision of counter-propagating pulses and vortices was studied by Sakaguchi et al. [26]. The results showed that the acceleration occurs at the collisions of two counter-propagating one-dimensional pulse and two dimensional vortices. For a fixed set of parameters, it was observed that the moving pulses are accelerated and the energy increases at the moment of collision.

Unlike the QCSH equation described above, numerical simulations conducted specifically for the QCSH equation with the viscous term are still very limited. We review several numerical results with regards to this equation in the following.

A study was conducted using the Euler method to examine the dynamics of the dislocations in the aligned ordering striped system of the ordering kinetics for a 2D anisotropic Swift-Hohenerg model [24]. Numerical measurements showed that the average speeds for the motion of the dislocations obey power laws in time with different amplitudes but the same exponents. Moreover, the position and velocity distribution functions are only weakly anisotropic. In addition, the effect of viscosity for the motion of pulses was studied in [25, 27, 28]. It was found that the viscous term f determined the velocity of pulses. Motivated by the observation of localized circular (oscillations), Crawford and Riecke numerically investigated an extension of a Swift-Hohenberg model that exhibits a subcritical transition to square patterns [10]. Localized oscillon-type solutions were studied numerically using a pseudospectral code by first performing a weakly nonlinear analysis to obtain the periodic solutions. They concluded that oscillon-type structures are indeed a general feature in systems where the transition to squares is subcritical and the basic state Is sufficiently stable. The dissipative effects, namely the role of higher-order terms in spectral filtering in the case of passively mode-locked lasers modeled by the QCSH equation was explained in [30]. First, the QCSH equations with viscous terms has a greater variety of solutions than the QCSH equations without viscous terms. Second, its composite stationary and moving pulses are generated for a wider range of parameters due to the more complicated spectral response. Finally. three different types of bound soliton states were also found namely: plain pulses, composite pulse, and narrow composite pulse.

As we noted earlier on, there has been considerable interest whether the stable spatially localized states could be found in the QCSH equation ever since this property was previously observed in the subcritical complex Ginzburg-Landau equation. Thus it is very important to have an efficient and accurate numerical method that can explain this phenomena. To our knowledge, there are not many numerical simulation results presented so far that can explain the effect of the additional viscous term and the behavior of localized states observed in the QCSH equation. Very few numerical studies are directed at the QCSH equation (we note that a finite difference scheme has been proposed for the Swift-Hohenberg equation with strict implementation of Lyapunov Functional in [11]). We therefore propose an efficient solver for the equation–the time splitting Fourier pseudospectral method in order to examine this. Our numerical method is based on discretizing the spatial derivatives by the Fourier pseudospectral method and applying the second-order Strang splitting method for the time derivatives. The method has been demonstrated to be very efficient and accurate for solving the nonlinear Schrödinger-type equations (see for example [5–7] and their reference inside). In this paper we want to show that the method is also an efficient solver for the QCSH equation.

The rest of the paper is organized as follows: In Section 2, we investigate some dynamical properties of the QCSH equation. In Section 3, we propose two different time-splitting Fourier pseudospectral methods to numerically solve the QCSH equation. In Section 4, we show the method's numerical accuracy both in time and space. We also apply the method to study one-soliton dynamics and two-soliton dynamics. Generated of stable moving pulses in one dimension (1D) and stable vortex solitons in two dimensions (2D) are reported. Finally conclusions are drawn in Section 5.

2. Dynamical properties of the Swift-Hohenberg equation

There are many important quantities in studying the QCSH equation (1.1). One of them is the norm defined as

$$N(t)=\int |\psi(\mathbf{x},t)|^2 d\mathbf{x}, \quad t\geq 0. \tag{2.1}$$

Taking the derivative with respect to time t gives us

$$\frac{dN}{dt}=2\mathrm{Im}\left(\int \left(a|\psi|^2+b|\psi|^4+c|\psi|^6-d|\nabla\psi|^2+f|\triangle\psi|^2\right)\, d\mathbf{x}\right). \tag{2.2}$$

If the parameters a,b,c,d,e, and f are real, then the norm N is conserved since $\frac{dN}{dt}=0$; if the parameters b,c,d,e, and f are real, then the norm N will increase (decrease) with respect to time t when a is a positive (negative) imaginary number.

Another quantity is the momentum defined as

$$P=i\int \left(\bar{\psi}\nabla\psi-\psi\nabla\bar{\psi}\right) d\mathbf{x}=2\mathrm{Im}\left(\int \psi\nabla\bar{\psi}\, d\mathbf{x}\right),\ t\geq 0. \tag{2.3}$$

From the QCSH equation, we have

$$\frac{dP}{dt}=4\mathrm{Im}\left(\int \left([a\psi+b|\psi|^2\psi+c|\psi|^4\psi+d\triangle\psi+f\triangle^2\psi]\nabla\bar{\psi}\right)\, d\mathbf{x}\right). \tag{2.4}$$

When a,b,c,d,f are real variable, the energy defined as follows is also an important quantity governed by the QCSH equation with real coefficients:

$$E(\psi)=\left(\int \left(a|\psi|^2+\frac{b|\psi|^4}{2}+\frac{c|\psi|^6}{3}-d|\nabla\psi|^2+f|\triangle\psi|^2\right)\, d\mathbf{x}\right). \tag{2.5}$$

It is conserved since $\frac{dE}{dt}=0$.

When $f=0$, the QCSH equation collapses into the QCGL as we noted earlier. We have the following lemma for the QCGL equation:

Lemma 2.1. *Suppose that $\phi_0(\mathbf{x})$ is a solution of the equation*

$$\omega\phi=a\phi+b|\phi|^2\phi+c|\phi|^4\phi+d\triangle\phi. \tag{2.6}$$

Then the QCSH equation (1.1) *with $f=0$ admits a soliton solution*

$$\phi_0(\mathbf{x}+dt\vec{v})e^{i\vec{v}(\mathbf{x}+dt\vec{v})-i\omega t}, \tag{2.7}$$

where ω is some constant and $\vec{v}$, the moving velocity of the soliton is some constant vector.

One can easily get the proof of this Lemma by substituting (2.7) into the QCSH equation (1.1) with $f=0$. Though it is difficult to construct a soliton-like solution as (2.7) for the QCSH equation, Maruno *et al.* obtain many exact soliton solutions for the one-dimensional Swift-Hohenberg equation. In Section 4, we will present some numerical simulations on soliton dynamics. In the next section, we develop an efficient numerical method for solving the QCSH (1.1).

3. Numerical methods for the Swift-Hohenberg equation

In this section, we present a time-splitting Fourier pseudospectral method to study the time evolution of the QCSH equation. For simplicity of notation, the method is introduced for the case of one space dimension. Generalizations to higher dimensions are straightforward for tensor product grids and the results remain valid without modifications. For d=1, the problems becomes

$$i\frac{\partial \psi}{\partial t} = a\psi + b|\psi|^2\psi + c|\psi|^4\psi + d\partial_{xx}\psi + f\partial_{xxxx}\psi, \qquad p \le x \le q,\ t > 0, \tag{3.1}$$

$$\psi(x, t=0) = \psi_0(x),\ p \le x \le q,\ \psi(p,t) = \psi(q,t) = 0, \qquad t \ge 0, \tag{3.2}$$

with $|p|$ and q sufficiently large.

We choose the spatial mesh size as $\triangle x = (q-p)/M > 0$, with M being an even positive integer, and the time step $\triangle t > 0$. The grid points and time sequence can be defined as

$$x_j = p + j\triangle x,\ j = 0, 1, \cdots, M; \qquad t_n = n\triangle t,\ n = 0, 1, 2, \cdots. \tag{3.3}$$

We denote ψ_j^n be the numerical approximation of $\psi(x_j, t_n)$.

3.1. A three-step splitting method

From time $t = t_n$ to $t = t_{n+1}$, Eq. (3.1) can be solved in two splitting steps. One first solves

$$i\frac{\partial \psi}{\partial t} = a\psi + d\partial_{xx}\psi + f\partial_{xxxx}\psi \tag{3.4}$$

for one time step, followed by solving

$$i\frac{\partial \psi}{\partial t} = b|\psi|^2\psi + c|\psi|^4\psi \tag{3.5}$$

for another time step.

To solve Eq. (3.4), we assume that

$$\psi(x,t) = \sum_{l=-M/2}^{M/2-1} \hat{\psi}_l(t) e^{i\mu_l(x_j - p)}, \tag{3.6}$$

where $\hat{\psi}_l(t)$ is the Fourier coefficient for the l^{th} mode, and

$$\mu_l = \frac{2\pi l}{q-p}, \qquad l = -\frac{M}{2}, \cdots, 0, \cdots, \frac{M}{2} - 1.$$

Plugging (3.6) into Eq. (3.4), we obtain

$$\frac{d\hat{\psi}_l(t)}{dt} = \hat{\psi}_l(t)\left[-i(a - d\mu_l^2 + f\mu_l^4)\right], \qquad l = -\frac{M}{2}, \cdots, 0, \cdots, \frac{M}{2} - 1. \tag{3.7}$$

Solving the above equation gives us

$$\hat{\psi}_l(t) = \hat{\psi}_l(t_n)\exp\left[-i(a - d\mu_l^2 + f\mu_l^4)(t - t_n)\right], \tag{3.8}$$

and then plugging (3.8) into (3.6), we get the solution of (3.4) as

$$\psi(x_j, t) = \sum_{l=-M/2}^{M/2-1} \hat{\psi}_l(t_n)\exp\left[-i(a - d\mu_l^2 + f\mu_l^4)(t - t_n)\right] e^{i\mu_l(x_j - p)}. \tag{3.9}$$

For $t \in [t_n, t_{n+1}]$, multiplying (3.5) by $\overline{\psi(x,t)}$ we get

$$i\psi_t\overline{\psi(x,t)} = b|\psi(x,t)|^4 + c|\psi(x,t)|^6. \tag{3.10}$$

Taking conjugate on both sides, the above equation becomes

$$-i\overline{\psi_t}\psi(x,t) = \bar{b}|\psi(x,t)|^4 + \bar{c}|\psi(x,t)|^6. \tag{3.11}$$

Subtracting (3.11) from (3.10) and multiplying by -i, we get the following ordinary differential equation for $\rho = |\psi(x,t)|^2$:

$$\partial_t\rho = 2[\mathrm{Im}(b)\rho + \mathrm{Im}(c)\rho^2]\rho = 2g(\rho)\rho \tag{3.12}$$

with the function $g(\rho) = \mathrm{Im}(b)\rho + \mathrm{Im}(c)\rho^2$.

To solve (3.12), we define

$$r(s) = \int \frac{1}{sg(s)}ds, \quad h(s,\tau) = \begin{cases} r^{-1}(r(s) - 2\tau), & s > 0, \tau \geq 0, \\ 0, & s = 0, \tau \geq 0. \end{cases} \tag{3.13}$$

If $g(s) \geq 0$ for $s \geq 0$, we find

$$0 \leq h(s,\tau) \leq s, \qquad \text{for } s \geq 0, \tau \geq 0,$$

and the solution of the ordinary differential equation (3.12) can be expressed by

$$\begin{aligned} 0 \leq \rho(t) &:= |\psi(x,t)|^2 = h(|\psi(x,t)|^2, t - t_n) \\ &\leq \rho(t_n) := |\psi(x,t_n)|^2, \qquad t_n \leq t \leq t_{n+1}. \end{aligned} \tag{3.14}$$

Combining (3.12) and (3.14), we obtain for $t \in [t_n, t_{n+1}]$,

$$i\psi_t = bh(|\psi(x,t_n)|^2, t - t_n)\psi(x,t) + c[h(|\psi(x,t_n)|^2, t - t_n)]^2\psi(x,t). \tag{3.15}$$

Integrating (3.15) from t_n to t, we find

$$\psi(x,t) = \psi(x,t_n)\exp\Big(-i\big(F(|\psi(x,t_n)|^2, t - t_n) + G(|\psi(x,t_n)|^2, t - t_n)\big)\Big), \tag{3.16}$$

where we have defined

$$F(s,r)=\int_0^r bh(s,\tau)\,d\tau\geq 0,\quad G(s,r)=\int_0^r c[h(s,\tau)]^2\,d\tau. \tag{3.17}$$

From $t=t_n$ to $t=t_{n+1}$, we combine the splitting steps via the second-order Strang splitting method, and we obtain the following three-step time-splitting Fourier pseudospectral method for the problem. The detailed algorithm of the method is given by

$$\psi_j^*=\psi_j^n\exp\{-i[F(|\psi_j^n|^2,\triangle t/2)+G(|\psi_j^n|^2,\triangle t/2)]\}, \tag{3.18}$$

$$\psi_j^{**}=\sum_{l=-M/2}^{M/2-1}\hat{\psi^*}_l\exp\left[-i(a-d\mu_l^2+f\mu_l^4)(t-t_n)\right]e^{i\mu_l(x_j-p)}, \tag{3.19}$$

$$\psi_j^{n+1}=\psi_j^{**}\exp\{-i[F(|\psi_j^{**}|^2,\triangle t/2)+G(|\psi_j^{**}|^2,\triangle t/2)]\}, \tag{3.20}$$

$$j=0,1,\cdots,M-1.$$

For Eq. (3.12), if both $\mathrm{Im}(b)$ and $\mathrm{Im}(c)$ are zero, then we can find that

$$F(s,r)=sr,\quad G(s,r)=s^2r.$$

If $\mathrm{Im}(b)=0$ and $\mathrm{Im}(c)\neq 0$, then we can find that

$$F(s,r)=\frac{-b}{\mathrm{Im}(c)}\left[\left(s^{-2}-4\mathrm{Im}(c)r\right)^{1/2}-s^{-1}\right],\quad G(s,r)=\frac{-c}{4\mathrm{Im}(c)}\ln|s^{-2}-4\mathrm{Im}(c)r|.$$

If $\mathrm{Im}(b)\neq 0$ and $\mathrm{Im}(c)=0$, then we can find that

$$F(s,r)=-\frac{b}{2\mathrm{Im}(b)}\ln|1-2\mathrm{Im}(b)sr|,\quad G(s,r)=-\frac{cs^2r}{1-2\mathrm{Im}(b)sr}.$$

However, if both $\mathrm{Im}(b)$ and $\mathrm{Im}(c)$ are nonzero, we cannot find the analytical form for the function $h(s,\tau)$ in (3.14) and, furthermore, we cannot get the explicit formulation for $F(s,r)$ and $G(s,r)$ in (3.16). Thus, in practice, we may use the fourth-order Runge-Kutta method to numerically solve the ordinary differential equation (3.12). In the following, we propose a new time-splitting method to solve the problem.

3.2. A five-step splitting method

As mentioned above, when both $\mathrm{Im}(b)$ and $\mathrm{Im}(c)$ are nonzero, Eq. (3.12) cannot be solved analytically. Therefore, we introduce another method which solves (3.1) in three splitting steps, i.e.,

$$i\frac{\partial\psi}{\partial t}=a\psi+d\partial_{xx}\psi+f\partial_{xxxx}\psi, \tag{3.21}$$

$$i\frac{\partial\psi}{\partial t}=b|\psi|^2\psi. \tag{3.22}$$

$$i\frac{\partial\psi}{\partial t}=c|\psi|^4\psi. \tag{3.23}$$

The solution of (3.21) is given by (3.6), while for (3.22) and (3.23), we can use the similar procedure to get their exact solutions. For (3.22), we have for $t \in [t_n, t_{n+1}]$,

$$\psi(t) = \begin{cases} \psi^n \exp\{-iRe(b)|\psi^n|^2(t-t_n)\}, & \mathrm{Im}(b) = 0, \\ \dfrac{\psi^n}{\sqrt{|1-2\mathrm{Im}(b)|\psi^n|^2(t-t_n)|}} & \\ \quad \times \exp\left\{ i\dfrac{Re(b)}{2\mathrm{Im}(b)} \ln|1-2\mathrm{Im}(b)|\psi^n|^2(t-t_n)| \right\}, & \text{otherwise.} \end{cases} \tag{3.24}$$

Similarly, solving (3.23) gives us

$$\psi(t) = \begin{cases} \psi^n \exp\{-iRe(b)|\psi^n|^4(t-t_n)\}, & \mathrm{Im}(b) = 0, \\ \dfrac{\psi^n}{|1-4\mathrm{Im}(b)|\psi^n|^4(t-t_n)|^{1/4}} & \\ \quad \times \exp\left\{ i\dfrac{Re(b)}{4\mathrm{Im}(b)} \ln|1-4\mathrm{Im}(b)|\psi^n|^4(t-t_n)| \right\}, & \text{otherwise.} \end{cases} \tag{3.25}$$

Thus we can combine (3.6), (3.24) and (3.25) by the second-order Strang splitting method, we get the following five-step splitting method, i.e., from time $t = t_n$ to $t = t_{n+1}$,

(i) evolve (3.24) for half time step $\triangle t/2$ with the initial data ψ^n given at $t = t_n$;

(ii) evolve (3.25) for half time step $\triangle t/2$ with the new data obtained in (i);

(iii) evolve (3.6) for the time step $\triangle t$ with the new data obtained in (ii);

(iv) evolve (3.25) for half time step $\triangle t/2$ with the new data obtained in (iii);

(v) evolve (3.24) for half time step $\triangle t/2$ with the new data obtained in (iv) and obtain ψ^{n+1}.

The detailed algorithm is as follows:

$$\psi_j^{(1)} = \begin{cases} \psi_j^n \exp\{-iRe(b)|\psi_j^n|^2\triangle t/2\}, & \mathrm{Im}(b) = 0, \\ \dfrac{\psi^n}{\sqrt{|1-\mathrm{Im}(b)|\psi_j^n|^2\triangle t|}} \exp\left\{ i\dfrac{Re(b)}{2\mathrm{Im}(b)} \ln|1-\mathrm{Im}(b)|\psi_j^n|^2\triangle t| \right\}, & \text{otherwise.} \end{cases}$$

$$\psi_j^{(2)} = \begin{cases} \psi^n \exp\{-iRe(b)|\psi_j^{(1)}|^4\triangle t/2\}, & \mathrm{Im}(b) = 0, \\ \dfrac{\psi^n}{|1-2\mathrm{Im}(b)|\psi_j^{(1)}|^4\triangle t|^{1/4}} \exp\left\{ i\dfrac{Re(b)}{4\mathrm{Im}(b)} \ln|1-2\mathrm{Im}(b)|\psi_j^{(1)}|^4\triangle t| \right\}, & \text{otherwise.} \end{cases}$$

$$\psi_j^{(3)} = \sum_{l=-M/2}^{M/2-1} \hat{\psi^{(2)}}_l \exp\left[-i(a - d\mu_l^2 + f\mu_l^4)(t-t_n) \right] e^{i\mu_l(x_j - p)},$$

$$\psi_j^{(4)} = \begin{cases} \psi^n \exp\{-iRe(b)|\psi_j^{(3)}|^4 \triangle t/2\}, & \text{Im}(b) = 0, \\ \dfrac{\psi^n}{|1-2\text{Im}(b)|\psi_j^{(3)}|^4 \triangle t|^{1/4}} \exp\left\{ i \dfrac{Re(b)}{4\text{Im}(b)} \ln|1-2\text{Im}(b)|\psi_j^{(3)}|^4 \triangle t| \right\}, & \text{otherwise.} \end{cases}$$

$$\psi_j^{n+1} = \begin{cases} \psi_j^n \exp\{-iRe(b)|\psi_j^{(4)}|^2 \triangle t/2\}, & \text{Im}(b) = 0, \\ \dfrac{\psi^n}{\sqrt{|1-\text{Im}(b)|\psi_j^{(4)}|^2 \triangle t|}} \exp\left\{ i \dfrac{Re(b)}{2\text{Im}(b)} \ln|1-\text{Im}(b)|\psi_j^{(4)}|^2 \triangle t| \right\}, & \text{otherwise.} \end{cases}$$

$$j = 0, 1, \cdots, M-1. \tag{3.26}$$

4. Numerical results

In this section we apply the proposed time-splitting Fourier pseudospectral method (3.26) to solve the one-dimensional and two-dimensional QCSH equations respectively. First, we test the numerical accuracy of the method. Second, we study how the viscous term f affects the dynamics of moving solitons. Finally, we investigate stable moving pulses and vortex solitons governed by the QCSH equation.

4.1. Accuracy tests in 1D

To examine the numerical accuracy of our numerical method in 1D, we use it to solve the 1D QCSH equation. The parameters are chosen as: $a = -0.075i$, $b = -1+2i$, $c = 0.5$, $d = -0.2-0.05i$, and $f = -0.025i$. The initial conditions is taken to be $\psi(x, t=0) = \frac{1}{2}\text{sech}(x)$.

We solve the problem in the interval $[-64, 64]$, i.e. $p = -64$ and $q = 64$ with a homogenous boundary condition.We compute a numerical solution with a very fine mesh, e.g. $\triangle x = \frac{128}{4096}$, and a very small time step $\triangle t = 0.0001$, as the 'exact' solution ψ^e. Let $\psi^{\triangle x, \triangle t}$ denote the numerical solution under mesh size $\triangle x$ and time step $\triangle t$.

Firstly we test the spectral accuracy of the TSFP method in space. Table 1 shows the errors $||\psi^e(t) - \psi^{\triangle x, \triangle t}||_{l^2}$ at $t = 1.0$ with $\triangle t = 0.0001$ for different $\triangle x$.

Table 1: Spatial error analysis for TSFP: errors $||\psi^e(t) - \psi^{\triangle x, \triangle t}||_{l^2}$ at $t = 1.0$ with $\triangle t = 0.0001$.

$\triangle x$	1	1/2	1/4	1/8	1/16
Error	0.1763	6.6405E-4	9.7748E-8	1.8626E-8	3.3886E-13

Table 2: Temporal error analysis for TSFP: errors $||\psi^e(t) - \psi^{\triangle x, \triangle t}||_{l^2}$ at $t = 1.0$ with $\triangle x = 1/32$.

$\triangle t$	$\frac{1}{32}$	$\frac{1}{64}$	$\frac{1}{128}$	$\frac{1}{256}$	$\frac{1}{512}$
Error	2.1385E-4	5.4085E-5	1.3595E-5	3.4048E-6	8.4976E-7

Subsequently, we test the accuracy of TSFP in time. Table 2 shows the errors $||\psi(t) - \psi^{\triangle x,\triangle t}||_{l^2}$ at $t = 1.0$ with $M = 4096$ for different $\triangle t$.

From Tables 1 and 2, we can conclude that the numerical method–TSFP has spectral order accuracy for spatial derivatives and the second-order accuracy for time derivatives in 1D.

4.2. Dynamics of one soliton in 1D

In this subsection, our goal is to observe the effect of the additional viscous term f in the dynamics of one soliton. In the examples presented below, the values of the parameters used are $a = -0.04i$, $b = -1 + 0.04i$, $c = -0.008i$, and $d = -0.5$. The initial condition is set to be $\psi(x, t = 0) = 1.5\text{sech}[1.5(x - x_0)]e^{iv_0x}$. We study three cases: Case I: $x_0 = 0$

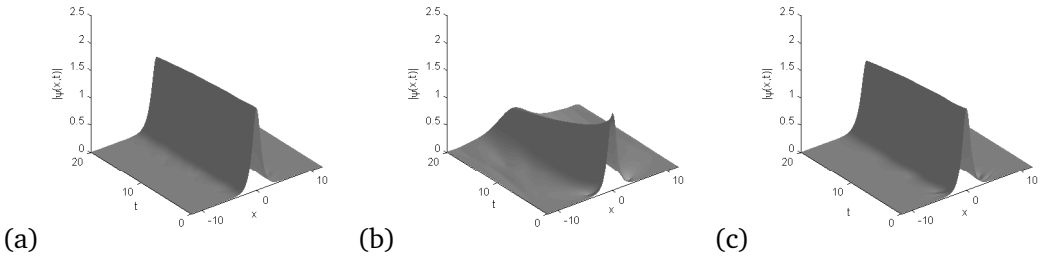

(a) (b) (c)

Figure 1: The dynamics of one soliton for case I. (a) $f = 0$; (b) $f = -0.05i$; (c) $f = 0.0025$.

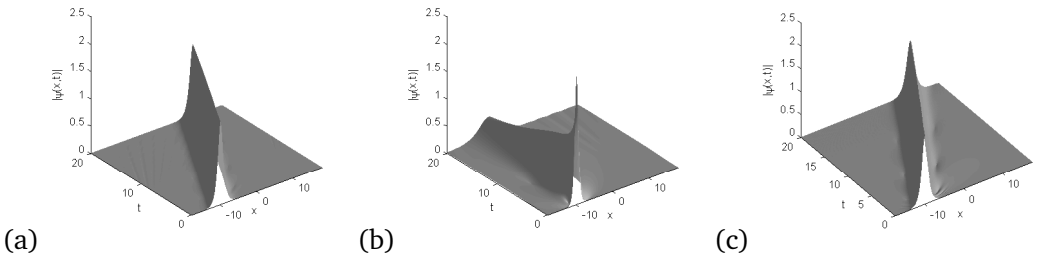

(a) (b) (c)

Figure 2: The dynamics of one soliton for case II. (a) $f = 0$; (b) $f = -0.05i$; (c) $f = 0.0025$.

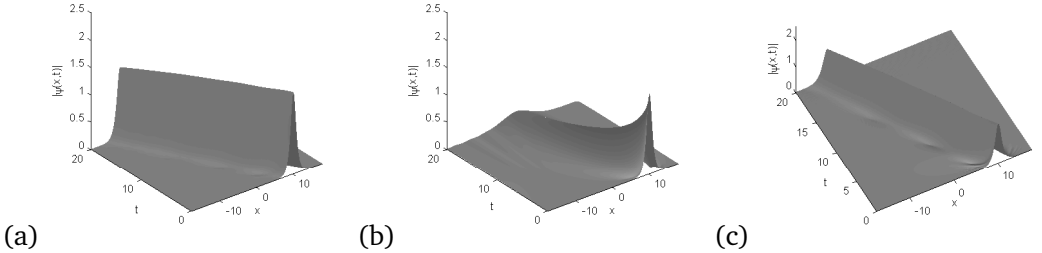

(a) (b) (c)

Figure 3: The dynamics of one soliton for case III. (a) $f = 0$; (b) $f = -0.05i$; (c) $f = 0.0025$.

and $v_0 = 0$; Case II: $x_0 = -10$ and $v_0 = 1$; Case III: $x_0 = 10$ and $v_0 = -1$.

In the numerical experiments, we set one soliton centered at the origin ($x_0 = 0$) with zero velocity $v_0 = 0$ initially in case I. When the viscous term f is zero, a moving soliton comes out, which has been shown in Fig. 1(a). We set one soliton centered at the position ($x_0 = -10$) with velocity $v_0 = 1$ initially in case II. In this case we have rightward-moving soliton, as shown in Fig. 2(a). We set one soliton centered at the position ($x_0 = 10$) with velocity $v_0 = -1$ initially in case III. In this case we have leftward-moving soliton, as shown in Fig. 3(a).

However, when the viscous term f becomes a negative imaginary number, the moving soliton may varnish, as shown in Fig. 1(b) or Fig. 2(b) or Fig. 3(b). When the viscous term f becomes a positive real number, the moving soliton keeps its form, as what can be seen in Fig. 1(c) or Fig. 2(c) or Fig. 3(c).

From the numerical results shown in Figs. 1, 2 and 3, two observations can be made:(1) The stable moving solitons can be found from the dynamics governed by the QCSH equation; (2) the viscous term f can tune the moving soliton on and off.

4.3. Dynamics of two solitons in 1D

In this subsection, our goal is to observe the effect of the additional viscous term f in the dynamics of two soliton. In the examples below, the values of the parameters used are $a = -0.04i$, $b = -1 + 0.04i$, $c = -0.008i$, and $d = -0.5$. The initial condition is set to be $\psi(x, t = 0) = 1.5\text{sech}[1.5(x - x_1)]e^{iv_1 x} + 1.5\text{sech}[1.5(x - x_2)]e^{iv_2 x}$. We study three cases: Case I, $x_1 = -18$ and $v_1 = 2.5$; $x_2 = -10$ and $v_2 = 0.5$; Case II, $x_1 = -18$ and $v_1 = 0.5$; $x_2 = -10$ and $v_2 = 2.5$; Case III, $x_1 = -8$ and $v_1 = 1$; $x_2 = 8$ and $v_2 = -1$.

We consider collisions between two moving solitons. With this in mind, in case I we prepare the initial condition with one soliton set at the position $x = -18$ with the velocity $v_1 = 2.5$, and the other one placed at $x = -10$ with the velocity $v_2 = 0.5$. The soliton placed at $x = -18$ moves rightward with larger velocity than the soliton placed at $x = -10$. In case II, we prepare the initial condition with one soliton set at the position $x = -18$ with the velocity $v_1 = 0.5$, and the other one placed at $x = -10$ with the velocity $v_2 = 2.5$. The soliton placed at $x = -18$ moves rightward with slower velocity than the soliton placed at $x = -10$. In this case the two solitons do not interact with each other. In case III, we prepare the initial condition with one soliton set at the position $x = -10$ with the velocity $v_1 = 1$, and the other one placed at $x = 10$ with the velocity $v_2 = -1$. The soliton placed at $x = -10$ moves rightward while the soliton placed at $x = 10$ moves leftward.

When the viscous term f is zero or f is purely positive, two moving soliton with velocity 2.5 and 0.5, interact with each other and move on with its original form, as what have been shown in Fig. 4(a) and Fig. 4(c) respectively. However, when the viscous term f becomes a negative imaginary number, these interacting solitons go on until they varnish, as what have been shown in Fig. 4(b). Similar observations can be found for case II and case III, as shown in Fig. 5 and Fig. 6, respectively, though we prepare different initial conditions with two solitons placed at different positions.

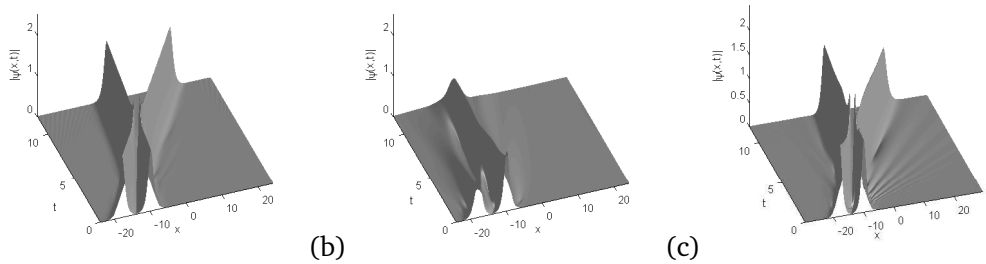

(a) (b) (c)

Figure 4: The dynamics of two moving solitons for case I. (a) $f = 0$; (b) $f = -0.05i$; (c) $f = 0.0025$.

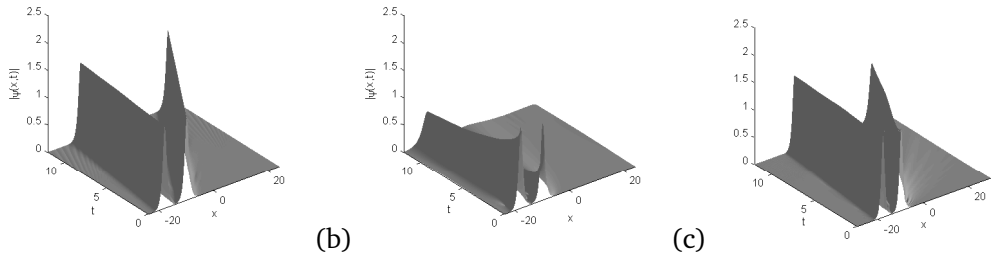

(a) (b) (c)

Figure 5: The dynamics of two moving solitons for case II. (a) $f = 0$; (b) $f = -0.05i$; (c) $f = 0.0025$.

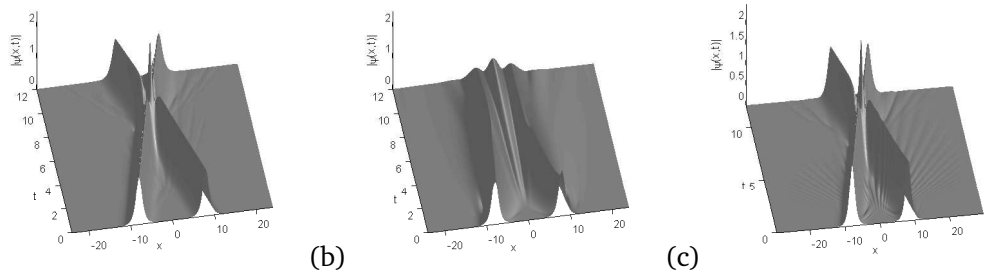

(a) (b) (c)

Figure 6: The dynamics of two moving solitons for case III. (a) $f = 0$; (b) $f = -0.05i$; (c) $f = 0.0025$.

4.4. Generation of stable moving pulses in 1D

In this subsection, our goal is to observe stable moving pulses. In the examples presented below, the values of the parameters used are $a = -0.05i$, $b = -1 + 1.6i$, $c = -0.1i$, and $f = -0.05i$.

Two different kinds of plain moving pulse are observed in Figs. 7(a) and 7(b). A composite moving pulse and wide composite moving pulse can be seen in Figs. 8(a) and 8(b), respectively. Similar observations were also obtained in [30,31].

Subsequently, we test the accuracy of TSFP in time. Table 4 shows the errors $||\psi(t) - \psi^{\triangle x,\triangle y,\triangle t}||_{l^2}$ at $t = 1.0$ with $M = 4096$ for different $\triangle t$.

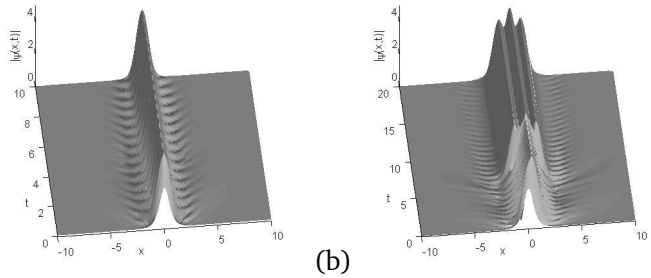

(a) (b)

Figure 7: The dynamics of plain moving pulses with $d = -0.5 + 0.05i$. (a) prepared with initial data $2.5\text{sech}(2.5x)$; (b) prepared with initial data $2.5\text{sech}(2.5x)e^{ix}$.

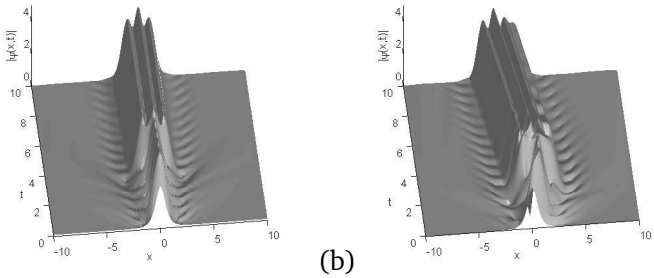

(a) (b)

Figure 8: The dynamics of composite moving pulses with $d = -0.5 - 0.05i$. (a) prepared with initial data $2.5\text{sech}(2.5x)$; (b) prepared with initial data $2.5\text{sech}(2.5x)e^{ix}$.

4.5. Accuracy tests in 2D

To examine the numerical accuracy of our numerical method in 2D, we use it to solve the 2D QCSH equation. The parameters are chosen as: $a = -0.04i$, $b = -1 + 0.04i$, $c = -0.008i$, $d = -0.5$, and $f = -0.05i$. The initial conditions is taken to be $\psi(x, y, t = 0) = 2.25\text{sech}(1.5x)\text{sech}(1.5y)$.

We solve the problem in the interval $[-8, 8] \times [-8, 8]$. We compute a numerical solution with a very fine mesh, e.g. $\triangle x = \triangle y = \frac{1}{32}$, and a very small time step $\triangle t = 0.0001$, as the 'exact' solution ψ^e. Let $\psi^{\triangle x, \triangle y, \triangle t}$ denote the numerical solution under mesh size $\triangle x$, $\triangle y$ and time step $\triangle t$.

Table 3: Spatial error analysis for TSFP: errors $||\psi^e(t) - \psi^{\triangle x, \triangle y, \triangle t}||_{l^2}$ at $t = 1.0$ with $\triangle t = 0.0001$.

$\triangle x = \triangle y$	1	1/2	1/4	1/8
Error	0.5054	1.7822E-4	3.6684E-7	9.2770E-8

Table 4: Temporal error analysis for TSFP: errors $||\psi^e(t) - \psi^{\triangle x, \triangle y, \triangle t}||_{l^2}$ at $t = 1.0$ with $\triangle x = \triangle y = 1/16$.

$\triangle t$	$\frac{1}{40}$	$\frac{1}{80}$	$\frac{1}{160}$	$\frac{1}{320}$	$\frac{1}{640}$
Error	0.0010	2.5388E-4	6.3537E-5	1.5877E-5	3.9577E-6

Firstly we test the spectral accuracy of the TSFP method in space. Table 3 shows the errors $||\psi^e(t) - \psi^{\triangle x,\triangle y,\triangle t}||_{l^2}$ at $t = 1.0$ with $\triangle t = 0.0001$ for different $\triangle x$.

From Tables 3 and 4, we can conclude that the numerical method–TSFP has spectral order accuracy for spatial derivatives and the second-order accuracy for time derivatives in 2D.

4.6. Generation of stable vortex solitons in 2D

Stable vortex solitons had been observed in the two-dimensional Ginzburg-Landau equation In this subsection, our goal is to observe whether we can observe the stable

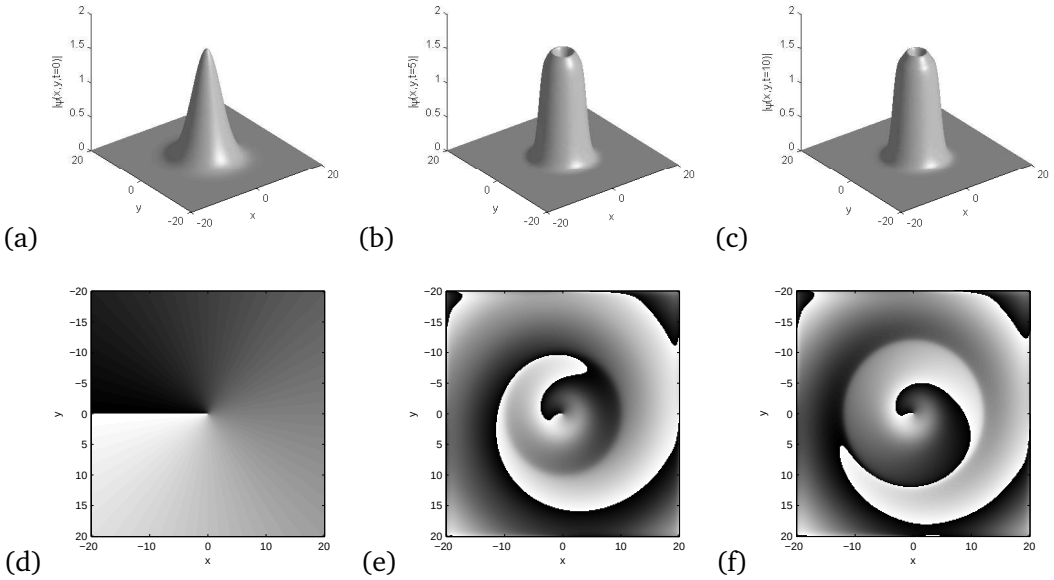

Figure 9: Generation of a stable vortex soliton prepared with initial data $\psi(x, y, t = 0) = 1.6e^{-(x^2+y^2)/25}e^{i\theta}$. Density plots for the wave function $|\psi(x, y, t)|$ at different times (a) t=0; (b) t=5; (c) t=10. Phase plots for the wave function $\psi(x, y, t)$ at different times; (d) t=0; (e) t=5; (f) t=10.

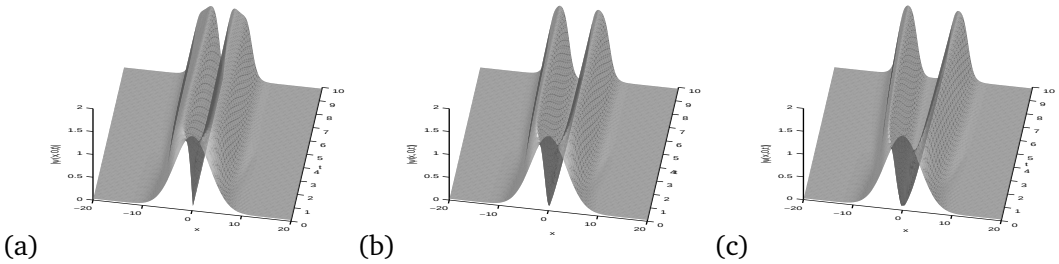

Figure 10: Density plots for the wave function $|\psi(x, 0, t)|$ at different times in the generation of stable vortex solitons. (a) case I; (b) case II; (c)case III.

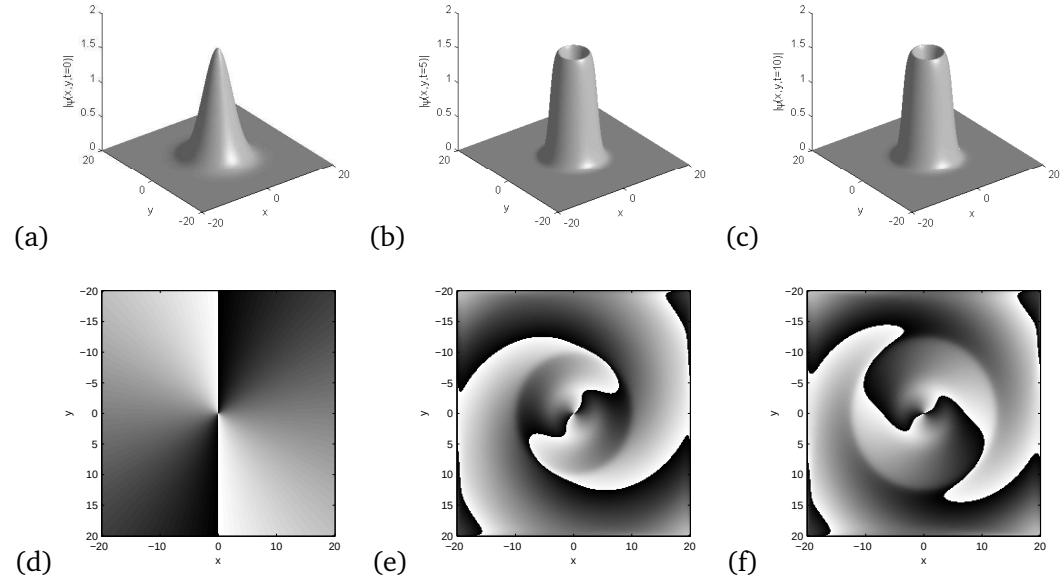

Figure 11: Generation of a stable vortex soliton prepared with initial data $\psi(x,y,t=0) = 1.6e^{-(x^2+y^2)/25}e^{i2\theta}$. Density plots for the wave function $|\psi(x,y,t)|$ at different times (a) t=0; (b) t=10; (c) t=10. Phase plots for the wave function $\psi(x,y,t)$ at different times (d) t=0; (e) t=5; (f) t=10.

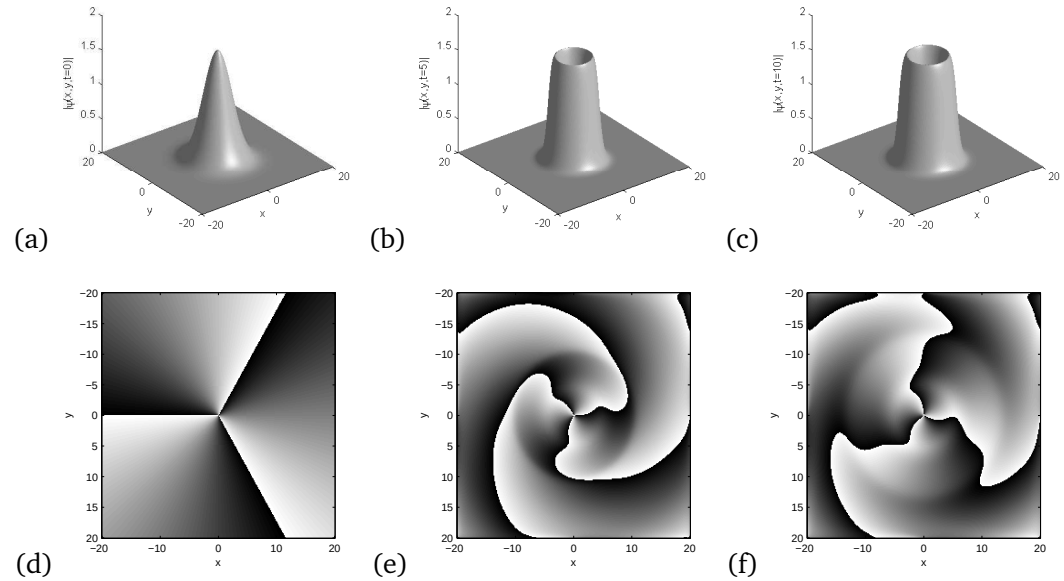

Figure 12: Generation of a stable vortex soliton prepared with initial data $\psi(x,y,t=0) = 1.6e^{-(x^2+y^2)/25}e^{i3\theta}$. Density plots for the wave function $|\psi(x,y,t)|$ at different times (a) t=0; (b) t=5; (c) t=10. Phase plots for the wave function $\psi(x,y,t)$ at different times (d) t=0; (e) t=5; (f) t=10.

vortex solitons in the QCSH. In the examples below, the values of the parameters used are $a = -0.5i$, $b = -1 + 2.5i$, $c = 0.1 - i$, $d = -0.5 + 0.05i$ and $f = -0.05$. We investigate three cases: Case I, $\psi(x, y, t = 0) = 1.6e^{-(x^2+y^2)/25}e^{i\theta}$; Case II, $\psi(x, y, t = 0) = 1.6e^{-(x^2+y^2)/25}e^{i2\theta}$; Case III, $\psi(x, y, t = 0) = 1.6e^{-(x^2+y^2)/25}e^{i3\theta}$ with $\theta = \arctan(y/x)$.

Stable vortex solitons are observed in Fig. 9, Fig. 11 and Fig. 12 respectively. In Fig. 10, we plot time evolution of the density of the wave function, i.e, $|\psi(x, 0, t)|$ at different times. From these figures, we can conclude that stable vortex solitons can be found in the two-dimensional QCSH equation.

5. Conclusions

We presented an efficient numerical method—the time-splitting Fourier pseudospectral method to discretize the quintic complex Swift-Hohenberg equation and showed that this method is very efficient and of spectral accuracy in space and second order accuracy in time for our problem as proven in our numerical accuracy test. We applied our numerical method to study the effect of the viscous term f in the quintic complex Swift-Hohenberg equation through the dynamics of one soliton and the interaction of two solitons. We found stable moving pulses and vortex solitons governed by the quintic complex Swift-Hohenberg equation.

Acknowledgments The research of H. Wang is supported in part by the Ministry of Education of Singapore grant No. R-146-000-120-112 and the National Natural Science Foundation of China grant No. 10901134. The authors thank very stimulating discussions with Professor Weizhu Bao in the subject. This work was partially done while the first author was visiting Department of Mathematics, National University of Singapore in 2010.

References

[1] G. P. Agrawal, Optical pulse propagation in doped fiber amplifiers, Phys. Rev. A, 44 (1991), pp. 7493.
[2] N. Akhmediev, A. S. Rodrigues, and G. E. Town, Interaction of dual-frequency pulsed in passively mode-locked lasers, Opt. Comm., 187(2001), pp. 419-426.
[3] N. Akhmediev, J. M. Soto-Crespo, and G. Town, Pulsating solitons, chaotic solitons, period doubling, and pulse coexistence in mode-locked lasers: complex Ginzburg-Landau equation approach, Phys. Rev. E, 63 (2001), pp. 056602.
[4] I. Aranson, D. Hochheiser, and J. V. Moloney, Boundary-driven selection of patterns in large-aspect-ratio lasers, Phys. Rev. A, 55(1997), pp. 3173.
[5] W. Bao and D. Jaksch, An explicit unconditionally stable numerical method for solving damped nonlinear Schrodinger equations with a focusing nonlinearity, SIAM J. Numer. Anal, 41(2003), pp. 1406-1426.
[6] W. Bao, S. Jin, and P. A. Markowich, On time-splitting spectral approximations for the Schrodinger equation in the semiclasslcal regime, J. Comput. Phys., 175 (2002), pp. 487-524.
[7] W. Bao and Y. Zhang, Dynamics of the ground state and central vortex states in Bose-Einstein condensation, Math. Mod. Meth. Appl. Sci., 15(2005), pp. 1863-1896.

[8] J. Burke and E. Knobloch, Localized states in the generalied Swift-Hollenberg equation, Phy. Rev. E. 73(2006), pp. 056211.
[9] G. Caginalp and P. C. Fife, Higher order phase field models and detailed anisotropv, Phys. Rev. B, 34(1986), pp. 4940-4943.
[10] C. Crawford and H. Riecke, Oscillon-type structures and their interactlon in a Swift-Hohenberg model, Physica D, 129(1999), pp. 83-92.
[11] C. I. Christov and J. Pontes, Numerical scheme for Swift-Hohenberg equation with strict implementation of Lyapunov Functional, Mathematical and Computer Modelling 35 (2002) 87-99.
[12] L.-C. Crasovan, B. A. Malomed, and D. Mihalache, Stable vortex solitons in the two-dimensional Ginzburg-Landau equation, Phys. Rev. E., 63, pp. 016605.
[13] G. T. Dee and W. Van Saarloos, Bistable systems with propagating fronts leading to pattern formation, Phys. Rev. Lett., 60(1988), pp. 2641-2644.
[14] R. A. Gardner and C. K. R. T. Jones, Travelling waves of a perturbed diffusion equation arising in a phase field model, Indiana Univ. Math. J, 38(1989), pp. 1197-1222.
[15] Q. Hat and G. F. Mazenb, Growth of order in an anlsotronlc Swift-Hohenberg model, Phys. Rev. E 73(2006), pp. 036117.
[16] H. Herrero and H. Riecke, Bound pairs of fronts in a real Ginzburg-Landau equation coupled to a mean field, Physica D, 85(1995), pp. 79-92.
[17] P. Kolodner, Drift, shape, and intrinsic destabillzation of pulses of traveling-wave convection, Phys. Rev, A, 44(1991), pp. 6448.
[18] Y. Kuramoto, Chemical oscillations, Waves and turbulence, Springer-Verlag, Berlin. 1984.
[19] J. Lega, J. V. Moloney, and A. C. Newell, Swift-Hohenberg equation for lasers, Phys. Rev Lett., 73(1994), pp. 2978.
[20] S. Longhi and A. Geraci, Swift-Hohenberz equation for optical parametrlc oscillators, Phys. Rev. A, 54(1996), pp. 4581.
[21] K. I. Maruno, A. Ankiewicz, and N. Akhmediev, Exact soliton solutions of the one-dimensional complex Swift-Hohenberg equation, Physica D, 176(2003), pp. 44-66.
[22] J. F. Mercier and J. V. Moloney, Derivation of semiconductor laser mean-field and Swift-Hohenberg equations,Phys. Rev. E, 66(2002), pp. 036221.
[23] L. A. Peletier and V. Rottschafer, Pattern selection of the solutions of the Swift-Hohenberg equation, Physica D, 194(2004), pp. 95-126.
[24] H. Qian and G. F. Mazenko, Growth of order in an anisotropic Swift-Hohenberg model, Phys. Rev. E, 73(2006), pp. 036117.
[25] H. Sakaguchi, Herringbone Pattern for an anisotropic complex Swift-Hohenberg equation, Phys. Rev. E, 58(1998), pp. 8021-8023.
[26] H. Sakaguchi, Motion of pulses and vortices in the cublc-quintic complex Ginzburg-Landau equation without viscosity, Physica D, 210(2005), pp. 138-148.
[27] H. Sakaguchi and H. R. Brand, Localized patterns for the quintic complex Swift-Hohenberg equation, Physica D, 117(1998), pp. 95-105.
[28] H. Sakaguchi and H. R. Brand, Stable localized solutions of arbitrary length for the quintic Swift-Hohenberg equation, Physica D, 97(1996), pp. 274-285.
[29] V. J. Sanchez-Morcillo, E. Rolddan, G. J. de Valcarcel, and K. Staliunas, Generalized complex Swift-Hohenberg equation for optical parametrlc oscillators, Phys. Rev., A, 56(1997), pp. 3237.
[30] J. M. Soto-Crespo and N. Akhmediev, Composite solitons and two-pulse generation in passively mode-locked lasers modeled by the complex quintic Swift-Hohenberg equation, Phys. Rev. E. 66(2002), pp. 066610.

[31] J. M. Soto-Crespo and N. Akhmediev, and V. V. Afansjev, Stability of the pulselike solutions of the quintic complex Ginzburg-Landau equation, J. Opt. Soc. Am. B, 13(1996), pp. 1439-1449.

[32] L. Yanti, Numerical studies of quintic complex Swift-Hohenberg equation, Thesis for the degree of Bachelor of Science with Honours, Department of Mathematics, National University of Singapore, 2007.